Available online at http://scik.org
Commun. Math. Biol. Neurosci. 2026, 2026:66
https://doi.org/10.28919/cmbn/9913
ISSN: 2052-2541

SIR MODEL ANALYSIS OF TRAFFIC CONGESTION DYNAMICS IN URBAN AREAS

NURCAHYA YULIAN ASHAR, R. HERU TJAHJANA*, MOCH. FANDI ANSORI

Department of Mathematics, Faculty of Science and Mathematics, Universitas Diponegoro, Semarang, 50275, Indonesia

Abstract. In highway traffic flows, where most vehicles pass over flyovers to bypass congestion at the macro level, there is a close relationship with the spread of infectious diseases, which are most commonly modeled using the susceptible-infected-recover(SIR) model. To smoothen traffic flow, a control variable is introduced that will be optimized, in this case, the duration of the green light at an intersection. Stability behavior of equilibrium points, reproduction number $\mathscr{R}_0$, and its effect on the three compartments. The numerical simulations were verified to confirm the previous results. The behavior of the three compartments with respect to the $\mathscr{R}_0$ value was obtained. The numerical simulation results also showed the positive impact of the duration of the green light on vehicles affected by traffic congestion.

Keywords: traffic congestion; stability analysis; basic reproduction number.

2020 AMS Subject Classification: 37N25, 37C75, 93B35.

1. Introduction

The SIR model and its modifications have been widely used in mathematical models such as [1], [2], [3], [4], [5], [6], [7], [8], [9], and [10]. In these studies, the model successfully produced expected results. The SIR model was then adapted to the traffic case from a macroscopic

*Corresponding author
E-mail address: redemtusherutjahjana@lecturer.undip.ac.id

Received April 07, 2026

perspective. In [11], the SIR model was introduced to reflect the dynamics of congestion spread in traffic networks. Simulations were conducted in six different metropolitan cities to obtain macro-scale congestion distribution patterns. The results of this study showed the existence of a basic reproduction number $\mathscr{R}_0$ in the spread of congestion in urban networks, which has characteristics similar to the reproduction number in infectious disease spread models. Furthermore, Wu et al. [12] modeled traffic congestion occurring at a node in a transportation network, where congestion can spread to the surrounding nodes. If not addressed immediately, congestion gradually develops and spreads to other points in the network. In this study, the SIR model proved to be capable of describing the dispersion of bottlenecks. Pu et al. [13] examined the dispersion of epidemic phenomena based on the SIR model in traffic networks by reviewing the influence of several factors, such as traffic load distribution and its level of homogeneity. The results showed that network density and load distribution homogeneity can accelerate the spread of epidemic congestion. Chen et al. [14] studied congestion spread patterns in traffic networks as an important part of network performance analysis. This study proposed the SIS-CP model, developed based on virus spread theory, to model density propagation patterns on large-scale networks. The SIS-CP model was found to be capable of optimally predicting the ratio of congested road sections, particularly during peak hours. In [15], an SIR model was developed for traffic congestion at simple intersection. An additional variable controlling the duration of the green lights was used to help reduce congestion. The behavior of the equilibrium points, numerical simulations, and sensitivity analysis of all existing variables are also discussed. The control variable had a positive impact, making it efficient for use under real-world conditions.

As the volume of vehicles increases every year and even every month in metropolitan cities, more and more roads are affected by moderate to severe congestion [16]. Owing to these conditions, a model is required that can be used to find alternative solutions so that congestion can be quickly resolved. In this case, the crucial point lies in the regulation of traffic lights so that there is no accumulation of the vehicles. However, in reality, there are still many traffic light settings in which the duration is only averaged out, so that traffic flow is not yet optimal. Controlling the duration of traffic lights at intersections is the key to avoiding congestion on a road section [16].

The SIR model is highly compatible for analyzing disease spread as well as traffic congestion, which can be viewed at both the macro- and micro-levels to describe patterns of congestion change. To the best of the authors' knowledge, previous studies have not discussed congestion on main roads consisting of regular lanes and flyovers with the green light duration parameter. The addition of a flyover scheme to the SIR model adapted to the problem of congestion was then proposed, and the effect of the green light duration parameter in helping to reduce congestion was checked. The proposed model relates to the conditions on a one-way road (without obstacles) with an overpass above it, where most vehicles pass through the overpass, and there is an intersection with traffic lights at the end of the road. The vehicle volume accumulates as the vehicle speed increases, particularly during rush hours. It is hoped that the behavior of traffic congestion will be clearly illustrated so that appropriate measures can be taken to degrade its level.

The stability behavior of the optimal SIR model is discussed in detail in this study. In Section 2, an SIR-based model is constructed that is adapted to existing traffic conditions, and the boundedness and positivity of the solution are checked, as well as the search for equilibrium points (non-endemic and endemic) and reproduction numbers. Section 3 continues the discussion in Section 2, namely, the analysis of the behavior of local and global equilibrium points. Section 4 illustrates the behaviors of the local and global equilibrium points. Section 3 continues the discussion in Section 2, namely, the analysis of the behavior of equilibrium points locally and globally. In Section 4, the numerical results are illustrated by considering several initial values and fixing the existing parameter values. Section 5 concludes the paper with a discussion.

2. MATHEMATICAL FORMULATION

Using the SIR model, which is often used in disease spread, the vehicle population at time $t \geq 0$ on a busy road section with an intersection with a green light was modeled. Three subpopulations are defined: $F(t)$, $C(t)$, and $R(t)$. $F(t)$ denotes the number of vehicles at risk of experiencing congestion at time t. $C(t)$ denotes the number of vehicles experiencing congestion at time t.

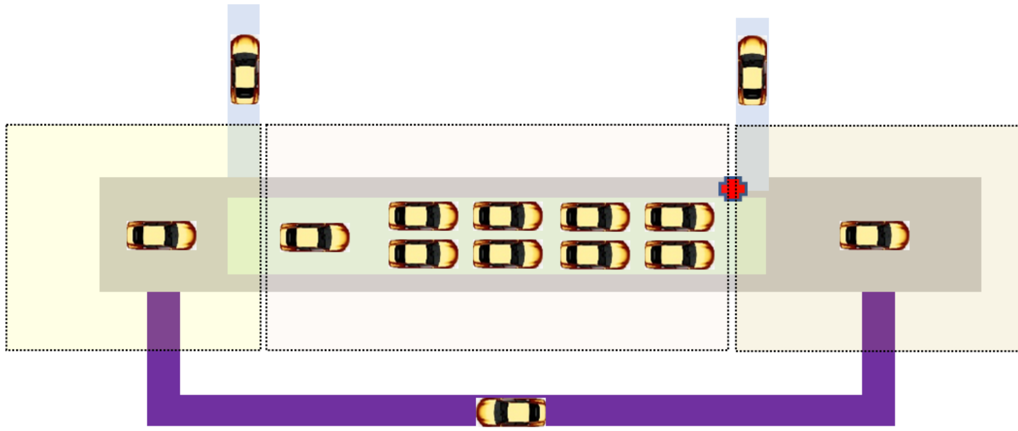

FIGURE 1. Illustration of A Road Section Modeled with The SIR Model

Fig. 1 illustrates a road section modeled using the SIR model. The main road section is gray, and the direct left-turn lane is light gray. The green lane indicates the presence of a flyover above the main gray road. The purple lane allows vehicles that have passed through congested areas to return to the vulnerable areas. There is a green plus-shaped traffic light and a buildup of vehicles before the intersection. The entire road is divided into three sections: the yellow section is the F population, the light pink section is the C population, and the brown section is the R population.

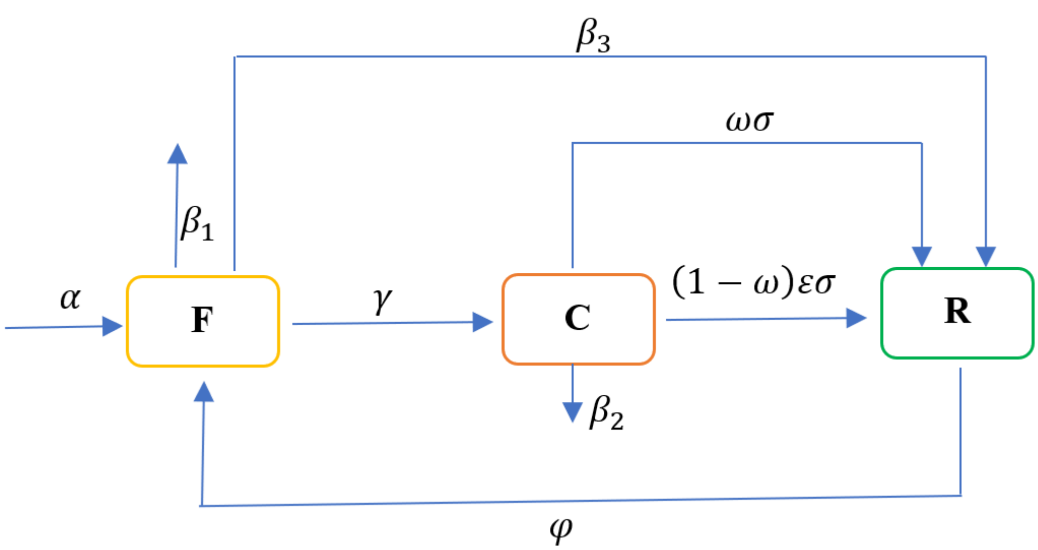

FIGURE 2. Compartment Diagram of The SIR Congestion Model

Parameter α in Fig. 2 represents the average speed of vehicles passing through the main road during the rush hour into the population $F(t)$. Furthermore, γ denotes the average speed of vehicles that experience congestion and transition from the population $F(t)$ to $C(t)$. A portion of vehicles entering the population $F(t)$ will exit the main road at an average rate of β_1. Most vehicles in $F(t)$ pass through the flyover at an average rate of β_3, directly entering population $R(t)$. Meanwhile, a small number of vehicles from the congested population $C(t)$ will immediately turn left at the intersection and exit $C(t)$ at an average rate of β_2. The parameter ε represents the proportion of green light duration within a traffic light cycle. Vehicles that obtain a green light will move from $C(t)$ to $R(t)$ at an average rate of σ. In addition, φ represents a small proportion of vehicles that return from $R(t)$ to the main road $F(t)$. This study also uses a parameter ω, which represents the duration of the green light allocated to alleviate congestion. Based on this framework, the system of differential equations of the SIR-type model is given by

$$
\begin{cases}
\dfrac{dF}{dt} = \alpha - (\beta_1 + \beta_3)F - \gamma FC + \varphi R, \\
\dfrac{dC}{dt} = \gamma FC - \beta_2 C - [\omega + (1-\omega)\varepsilon]\sigma C, \\
\dfrac{dR}{dt} = [\omega + (1-\omega)\varepsilon]\sigma C + \beta_3 F - \varphi R,
\end{cases}
\tag{1}
$$

with the initial conditions

$$F(0) \geq 0, \quad C(0) \geq 0, \quad R(0) \geq 0.$$

This section discusses the positivity and unboundedness of the solution, followed by the existence of endemic and non-endemic equilibrium points for fixed control parameter values ω. From system (1), we obtain in boundary set of R^3_+, $\dfrac{dF}{dt}(F=0) = \alpha + \varphi R > 0$, $\dfrac{dC}{dt}(C=0) \geq 0$, and $\dfrac{dR}{dt}(R=0) = [\omega + (1-\omega)\varepsilon]\sigma C + \beta_3 F \geq 0$. The solution will be pushed towards R^3_+ because all directions at the boundary are non-negative. Thus, the positivity of all variable solutions of system (1) for for all times $t > 0$ in this region is guaranteed.

We obtain the solutions that are bounded [17]. In the existing system, equation system (2) can be redefined by replacing variables F, C, R with P, C, R, where $P = F + \eta R$, and η is a constant that indicates the proportion of vehicles involved in the recovery process [18]. Using this transformation, the new system of equations is obtained as follows:

$$\begin{cases} \dfrac{dP}{dt} = \alpha - (\beta_1 + \beta_3)(P - \eta R) - \gamma(P - \eta R)C + \varphi R, \\ \dfrac{dC}{dt} = \gamma(P - \eta R)C - \beta_2 C - [\omega + (1-\omega)\varepsilon]\sigma C, \\ \dfrac{dR}{dt} = [\omega + (1-\omega)\varepsilon]\sigma C - \varphi R, \end{cases} \tag{2}$$

The phase space for this system is the quadrant $\mathbb{R}^3_+$, which consists only of values P, C, R that satisfy $P \geq 0, C \geq 0$, and $R \geq 0$. The following theorem shows that this system is well-defined (well-posed) and that the properties of this system also apply to the initial system.

Theorem 1. *Region D is defined as*

$$D = \left\{ (P, C, R) \in \mathbb{R}^3_+ | P + C + R \leq \frac{\alpha}{\beta^*} \right\}$$

is a positively invariant set for system (2).

Proof. To prove that the solutions of this system remain bounded, we examine the change in $\tilde{N}$, where $\tilde{N} = P + C + R$. The differential equation for $\tilde{N}$ can be calculated by summing the changes in each variable as follows:

$$\frac{d\tilde{N}}{dt} = \frac{dP}{dt} + \frac{dC}{dt} + \frac{dR}{dt}$$

By substituting the existing equations, we obtain an expression for $\dfrac{d\tilde{N}}{dt}$:

$$\frac{d\tilde{N}}{dt} = \alpha - (\beta_1 + \beta_3)P + (\beta_1 + \beta_3)\eta R - (\beta_2 + [\omega + (1-\omega)\varepsilon]\sigma)C.$$

The solution to this equation shows that $\tilde{N}(t)$ will not exceed $\dfrac{\alpha}{\beta^*}$ with $\beta^* = \min(\beta_1 + \beta_3, (\beta_1 + \beta_3)\eta, \beta_2 + [\omega + (1-\omega)\varepsilon]\sigma)$, which means that this system is bounded in a defined space. Therefore, the solution of this system remains within the positive invariant region, ensuring that P, C, and R do not increase without limit. Thus, this system ensures that the number of vehicles involved in congestion and recovery is always limited and stable in the positive space. $\square$

The equilibrium points are obtained by determining the solutions of

$$\frac{dF}{dt} = 0, \quad \frac{dC}{dt} = 0, \quad \text{and} \quad \frac{dR}{dt} = 0,$$

as follows:

$$\begin{cases} \alpha - (\beta_1 + \beta_3)F - \gamma FC + \varphi R = 0, \\ \gamma FC - \beta_2 C - [\omega + (1-\omega)\varepsilon]\sigma C = 0, \\ [\omega + (1-\omega)\varepsilon]\sigma C + \beta_3 F - \varphi R = 0, \end{cases} \tag{3}$$

The non-endemic equilibrium point is given by

$$E^0 = (F^0, C^0, R^0) = \left(\frac{\alpha}{\beta_1}, 0, \frac{\alpha\beta_3}{\varphi\beta_1}\right),$$

which is obtained by solving the system in (3). When the system reaches equilibrium at E_0, traffic congestion disappears. The basic reproduction number, $\mathscr{R}_0$, is defined as the number of secondary infections produced by one dense vehicle in a completely susceptible population. In [19], [20], the next-generation-matrix (NGM), $\mathscr{F}\mathscr{V}^{-1}$ method was used to find $\mathscr{R}_0$, where $\mathscr{R}_0$ is the spectral radius of the $\mathscr{F}\mathscr{V}^{-1}$ matrix at the equilibrium point E^0. In this case, $\mathscr{F}$ is the vector of new infections, while the transition matrix $\mathscr{V}$ represents the movement between compartments [21].

By $\mathscr{F} = \gamma F^0 = \dfrac{\alpha\gamma}{\beta_1}$, and $\mathscr{V}^{-1} = \left[\dfrac{1}{\beta_2 + [\omega + (1-\omega)\varepsilon]\sigma}\right]$ the basic reproduction number is given by

$$\mathscr{R}_0 = \frac{\alpha\gamma}{\beta_1\left(\beta_2 + \left[\omega + (1-\omega)\varepsilon\right]\sigma\right)}.$$

The endemic equilibrium point also can be determined from system (3) as follows

$$E^* = (F^*, C^*, R^*) = \left(\frac{\alpha}{\beta_1\mathscr{R}_0}, \frac{\alpha(\mathscr{R}_0 - 1)}{\mathscr{R}_0}, \frac{\alpha}{\varphi\mathscr{R}_0}\left(k\sigma(\mathscr{R}_0 - 1) + \frac{\beta_3}{\beta_1}\right)\right),$$

with $k = [\omega + (1-\omega)\varepsilon]\sigma$. We get if $\mathscr{R}_0 < 1$ if and only if $\beta_1\left(\beta_2 + \left[\omega + (1-\omega)\varepsilon\right]\sigma\right) > \alpha\gamma$, $F^* > 0$, and $C^*, R^* > 0$ if $\mathscr{R}_0 > 0$.

The endemic equilibrium exists only for $\mathscr{R}_0 > 1$. In Fig. 3, we show numerically that as $\mathscr{R}_0$ increases, F^* decreases monotonically, while C^* increases and approaches a saturation level. In contrast, R^* decreases with $\mathscr{R}_0$, indicating a redistribution of the population from the recovered class toward the endemic infected class as transmission intensity increases. These trends confirm that larger basic reproduction numbers promote persistent infections and shift the equilibrium structure.

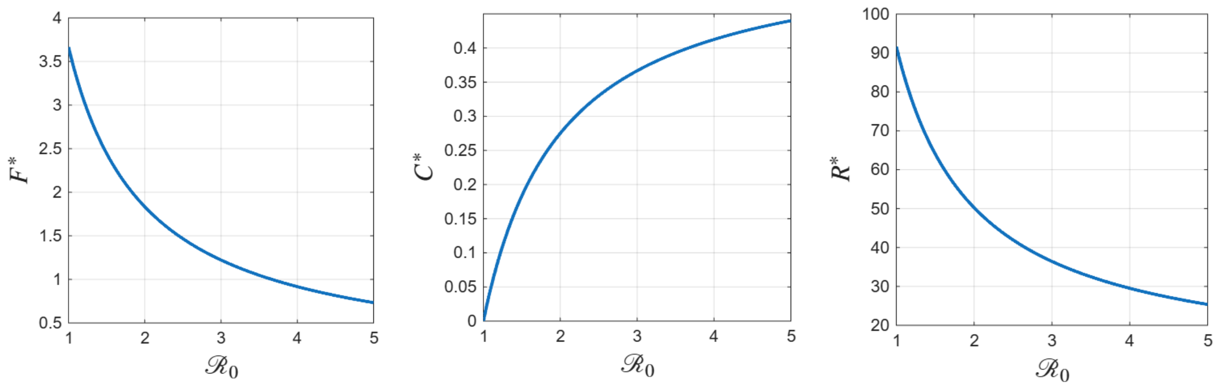

(A) F^* vs $\mathscr{R}_0$ (B) C^* vs $\mathscr{R}_0$ (C) R^* vs $\mathscr{R}_0$

FIGURE 3. Dependence of the endemic equilibrium components (F^*, C^*, R^*) on the basic reproduction number $\mathscr{R}_0$.

3. Stability Analysis

Stability at the congestion-free equilibrium point is investigated at E^0 for fixed control. System (1) is linearized at any point $E = (F, C, R)$, so that the Jacobian matrix corresponding to system (1) is

$$J(E) = \begin{pmatrix} -(\beta_1+\beta_3)-\gamma C & -\gamma F & \varphi \\ \gamma C & \gamma F - \beta_2 - [\omega + (1-\omega)\varepsilon]\,\sigma & 0 \\ \beta_3 & [\omega + (1-\omega)\varepsilon]\,\sigma & -\varphi \end{pmatrix}.$$

Next, the following stability theorem is established.

Theorem 2. *The non-endemic equilibrium E^0 is locally asymptotically stable if $\mathscr{R}_0 < 1$.*

Proof. The Jacobian matrix corresponding to system (1) is

$$J(E^0) = \begin{pmatrix} -(\beta_1+\beta_3) & -\gamma\left(\frac{\alpha}{\beta_1}\right) & \varphi \\ 0 & \gamma\left(\frac{\alpha}{\beta_1}\right) - \beta_2 - [\omega + (1-\omega)\varepsilon]\,\sigma & 0 \\ \beta_3 & [\omega + (1-\omega)\varepsilon]\,\sigma & -\varphi \end{pmatrix}.$$

The eigenvalues of the matrix $J(E^0) - \lambda I$ are $\lambda_1 = -(\beta_1+\beta_3)$, $\lambda_2 = \dfrac{\alpha\gamma}{\beta_1} - \beta_2 - k = (\beta_2 + k)(\mathscr{R}_0 - 1)$, and $\lambda_3 = -\varphi$, with $k = [\omega + (1-\omega)\varepsilon]\,\sigma$. It is clear that if $\mathscr{R}_0 < 1$, then λ_1, λ_2, and λ_3 are negative. Therefore, according to the Routh–Hurwitz stability criterion, the above theorem is fully proven. □

Theorem 3. *The endemic equilibrium E^* is locally asymptotically stable if $\mathscr{R}_0 > 1$.*

Proof. The Jacobian matrix corresponding to system (1) is

$$J(E^*) = \begin{pmatrix} -(\beta_1+\beta_3) - \dfrac{\gamma\alpha(\mathscr{R}_0 - 1)}{\mathscr{R}_0} & -\gamma\left(\dfrac{\alpha}{\beta_1\mathscr{R}_0}\right) & \varphi \\ \dfrac{\gamma\alpha(\mathscr{R}_0 - 1)}{\mathscr{R}_0} & \gamma\left(\dfrac{\alpha}{\beta_1\mathscr{R}_0}\right) - \beta_2 - k & 0 \\ \beta_3 & k & -\varphi \end{pmatrix},$$

where $k = [\omega + (1-\omega)\varepsilon]\sigma$.

The characteristic equation corresponding to $J(E^*)$ is

$$\lambda^3 + a_1\lambda^2 + a_2\lambda + a_3 = 0,$$

with coefficients

$$a_1 = (\beta_1+\beta_3) + \beta_2 + k + \varphi + \frac{\gamma\alpha(\mathscr{R}_0 - 1)}{\mathscr{R}_0} - \gamma\left(\frac{\alpha}{\beta_1\mathscr{R}_0}\right),$$

$$\begin{aligned} a_2 &= (\beta_1+\beta_3)(\beta_2+k+\varphi) + \varphi(\beta_2+k) \\ &\quad + \frac{\gamma\alpha(\mathscr{R}_0 - 1)}{\mathscr{R}_0}(\beta_2+k+\varphi) - \gamma\left(\frac{\alpha}{\beta_1\mathscr{R}_0}\right)(\beta_1+\beta_3+\varphi), \end{aligned}$$

$$a_3 = \varphi(\beta_1+\beta_3)(\beta_2+k) + \varphi\frac{\gamma\alpha(\mathscr{R}_0 - 1)}{\mathscr{R}_0}(\beta_2+k).$$

If $\mathscr{R}_0 > 1$, we get

$$a_1 > 0, a_2 > 0, a_3 > 0, a_1a_2 > a_3.$$

According to the Routh–Hurwitz stability criterion, all roots of the characteristic polynomial have negative real parts. Therefore, E^* is locally asymptotically stable when $\mathscr{R}_0 > 1$.

□

Theorem 4. *Non-endemic equilibrium E^0 of system* (1) *is globally asymptotically stable in the positively invariant region D whenever $\mathscr{R}_0 < 1$.*

Proof. Let $k = \left[\omega + (1-\omega)\varepsilon\right]\sigma > 0$. Consider the Lyapunov function

$$V(C) = C,$$

which is nonnegative in D and $V(C) = 0$ if and only if $C = 0$.

From the second equation of system (1), we obtain

$$\frac{dC}{dt} = C\left(\gamma F - (\beta_2 + k)\right).$$

Thus,

$$\dot{V} = \frac{dC}{dt} = C\left(\gamma F - (\beta_2 + k)\right).$$

Since the region D is bounded and positively invariant, we have

$$F(t) \leq F^0 = \frac{\alpha}{\beta_1}.$$

Therefore,

$$\dot{V} \leq C\left(\gamma F^0 - (\beta_2 + k)\right) = C(\beta_2 + k)(\mathscr{R}_0 - 1).$$

If $\mathscr{R}_0 < 1$, then

$$\dot{V} \leq -(\beta_2 + k)(1 - \mathscr{R}_0)C \leq 0,$$

and equality holds only when $C = 0$. Hence, $\dot{V}$ is negative definite with respect to C.

Every solution in D approaches the largest invariant set contained in

$$\{(F, C, R) \in D : \dot{V} = 0\} = \{(F, 0, R)\},$$

by the LaSalle's Invariance Principle.

On the invariant set $C = 0$, system (1) reduces to the linear subsystem

$$\frac{dF}{dt} = \alpha - (\beta_1 + \beta_3)F + \varphi R, \qquad \frac{dR}{dt} = \beta_3 F - \varphi R,$$

which has the unique equilibrium (F^0, R^0) and is globally asymptotically stable because its coefficient matrix is Hurwitz.

Therefore, the only invariant set in $\{\dot{V} = 0\}$ is E^0. By LaSalle's invariance principle, all trajectories in D converge to E^0. Hence, E^0 is globally asymptotically stable whenever $\mathscr{R}_0 < 1$. □

4. NUMERICAL SIMULATION

To illustrate the analytical results and qualitative behavior of the model, we perform numerical simulations of system (3). Unless otherwise stated, the initial conditions are chosen as

$$(F(0), C(0), R(0)) = (55, 5, 0).$$

The baseline parameter set is fixed at

$$\alpha = 0.55, \quad \beta_1 = 0.15, \quad \beta_2 = 0.35, \quad \beta_3 = 0.25, \quad \varphi = 0.01,$$

The transmission parameter for the subthreshold case is taken as $\gamma = 0.08$. We further select

$$\omega = 0.60, \qquad \varepsilon = 0.50, \qquad \sigma = 0.20,$$

which determines the effective transition rate in the recovered class.

Two simulation scenarios are shown in Fig. 4 are considered corresponding to $\mathscr{R}_0 < 1$ and $\mathscr{R}_0 > 1$, allowing us to compare the long-term dynamics below and above the epidemic threshold. When $\mathscr{R}_0 < 1$, the infected class $C(t)$ decays to zero, and the solution approaches the nonendemic equilibrium, indicating disease elimination. In contrast, when $\mathscr{R}_0 > 1$, $C(t)$ converges to a positive steady state, confirming the persistence of infection and convergence to the endemic equilibrium. These simulations illustrate the threshold role of $\mathscr{R}_0$ in determining the long-term dynamics.

The Partial rank correlation coefficient (PRCC) results in Fig. 5 shows that the congestion indicator $\mathscr{R}_0$ is most sensitive to the vehicle inflow rate α and the congestion transition rate γ, both of which have a strong positive influence. This indicates that a higher traffic arrival speed and faster formation of congestion significantly increase the risk of persistent traffic jams. In contrast, the exit rate β_1, left-turn discharge rate β_2, and clearance rate σ exhibit negative correlations, indicating that improved vehicle outflow and faster congestion release reduce $\mathscr{R}_0$. The control-related parameters ω and ε, which represent green light allocation and signal proportion, respectively, showed moderate positive effects, reflecting their role in regulating congestion dynamics. Overall, the sensitivity analysis highlights that traffic inflow and congestion formation dominate the system behavior, whereas efficient vehicle discharge and signal management act as stabilizing mechanisms.

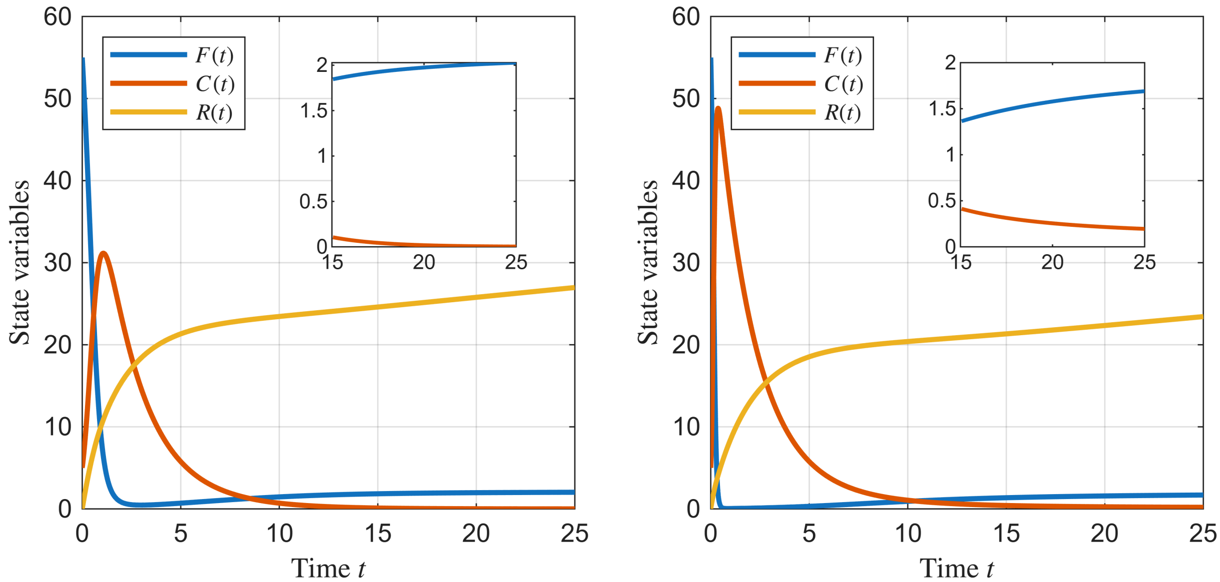

(A) $\mathscr{R}_0 < 1$ (B) $\mathscr{R}_0 > 1$

FIGURE 4. Time-series solutions of the system showing the threshold behavior governed by the basic reproduction number $\mathscr{R}_0$.

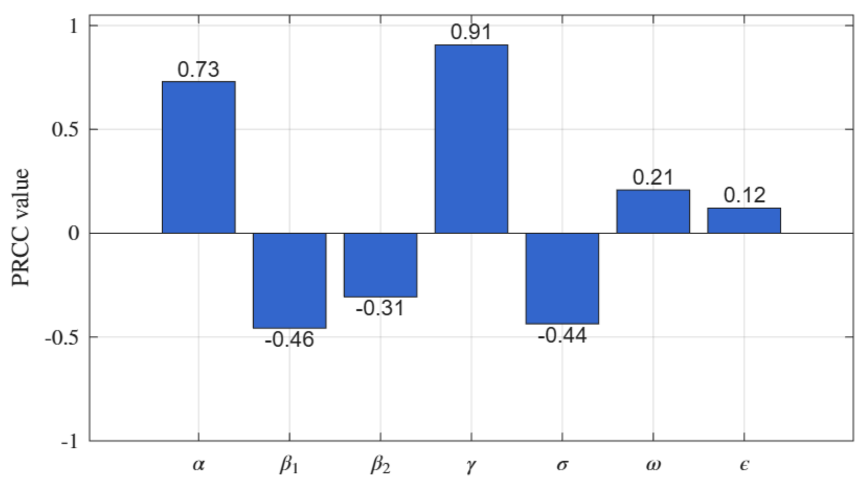

FIGURE 5. Partial rank correlation coefficients (PRCC) showing the sensitivity of the basic reproduction number $\mathscr{R}_0$ to model parameters.

The contour plots in Fig. 6 illustrate how the congestion threshold $\mathscr{R}_0$ depends on key parameter pairs. In the (γ, α) plane, $\mathscr{R}_0$ increases monotonically with both higher traffic inflow α and faster congestion formation γ, and the threshold curve $\mathscr{R}_0 = 1$ separates the regimes of dissipating and persistent congestion. Conversely, in the (β_2, σ) plane, larger exit and clearance rates reduce $\mathscr{R}_0$, shifting the system toward the subcritical region. These results confirm that congestion growth is driven by inflow and transition intensity, whereas efficient vehicle discharge and signal-induced clearance suppress sustained congestion.

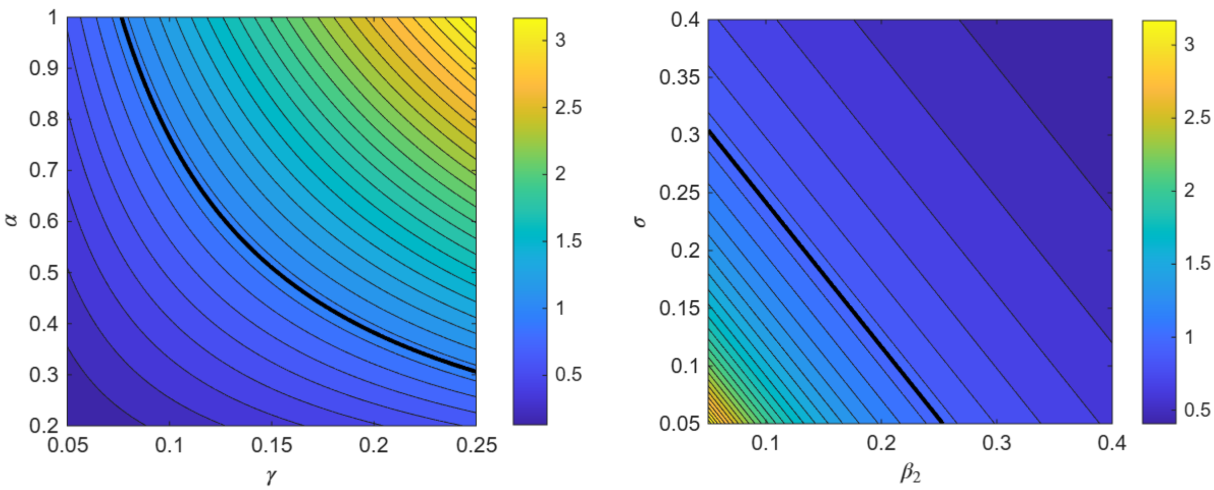

(A) (γ, α) plane

(B) (β_2, σ) plane

FIGURE 6. Contour plots of the congestion threshold $\mathscr{R}_0$. The bold curve represents $\mathscr{R}_0 = 1$, separating congestion regimes.

5. Discussion and Conclusion

This study used the susceptible-infected-recovered (SIR) model to analyze traffic congestion dynamics in urban areas, particularly on main roads equipped with flyovers. In this design, vehicles entering congested areas are considered susceptible populations, vehicles stuck in traffic are analogous to infected populations, and vehicles that have passed through congestion are considered recovered populations. Existing flyovers serve to reduce congestion by moving some vehicles to the upper lanes; however, there is still the potential for congestion at intersections. The duration of green lights at intersections is an important parameter that can reduce the basic reproduction number $\mathscr{R}_0$ and smooth traffic flow to prevent continuous congestion.

Next, the stability behavior of the non-endemic E^0 and endemic E^* equilibrium points in the system is explored. The non-endemic equilibrium point can indicate a congestion-free condition, where vehicles stuck in congestion eventually exit the system without causing sustained congestion. The asymptotic stability of the non-endemic equilibrium point is local and is achieved when the basic reproduction number $\mathscr{R}_0 < 1$. Conversely, the endemic equilibrium point is locally asymptotically stable when $\mathscr{R}_0 > 1$, which means that congestion will continue and reach an equilibrium state in which the number of vehicles stuck in congestion remains stable for a long time. Globally, the stability of the equilibrium point E^0 is asymptotic when $\mathscr{R}_0 < 1$.

The results of the numerical simulations and sensitivity analyses show the significant influence of all parameters on congestion dynamics. When $\mathscr{R}_0 > 1$, vehicles stuck in congestion $C(t)$ remain at higher values, indicating sustained congestion. Conversely, when $\mathscr{R}_0 < 1$, the number of vehicles stuck in congestion decreases until it reaches a congestion-free equilibrium. In addition, the sensitivity analysis shows that the congestion transition parameter γ has the strongest positive influence on $\mathscr{R}_0$, whereas the vehicle exit rate parameter β_1 shows the highest negative correlation, which means that an increase in this parameter can reduce the value of $\mathscr{R}_0$ and help ease congestion.

It can be concluded that congestion cases can be well modeled using the SIR. The local and global stability behaviors of the non-endemic and endemic equilibrium points can be clearly described. Numerical simulations show that the value of $\mathscr{R}_0$ significantly affects the population $C(t)$. The parameter of the duration of traffic lights will reduce congestion, although the parameters γ and β_1 play a more vital role.

Acknowledgement

This study was supported by funding sources Selain APBN FSM Undip with number 31.B/UN7.F8/PP/II/2026.

Conflict of Interests

The authors declare that there is no conflict of interests.

REFERENCES

[1] J. Nainggolan, M.F. Ansori, H. Tasman, An Optimal Control Model with Sensitivity Analysis for COVID-19 Transmission Using Logistic Recruitment Rate, Healthc. Anal. 7 (2025), 100375. https://doi.org/10.1016/j.health.2024.100375.

[2] R. Mahardika, Widowati, Y.D. Sumanto, Routh-Hurwitz Criterion and Bifurcation Method for Stability Analysis of Tuberculosis Transmission Model, J. Phys.: Conf. Ser. 1217 (2019), 012056. https://doi.org/10.1088/1742-6596/1217/1/012056.

[3] L. Alhusna, R. Herdiana, T. Udjiani, Kontrol Optimal Model Dinamik Penyebaran Penyakit Tuberkulosis dengan Kekambuhan di Kota Semarang, Limits: J. Math. Its Appl. 22 (2025), 217–236. https://doi.org/10.12962/limits.v22i3.4349.

[4] Sutimin, R. Herdiana, R.H. Soelistyo U, A.H. Permatasari, Stability Analysis of Tuberculosis Epidemic Model with Saturated Infection Force, E3S Web Conf. 202 (2020), 12023. https://doi.org/10.1051/e3sconf/202020212023.

[5] I. Cooper, A. Mondal, C.G. Antonopoulos, A SIR Model Assumption for the Spread of COVID-19 in Different Communities, Chaos Solitons Fractals 139 (2020), 110057. https://doi.org/10.1016/j.chaos.2020.110057.

[6] N.A. Kudryashov, M.A. Chmykhov, M. Vigdorowitsch, Analytical Features of the SIR Model and Their Applications to COVID-19, Appl. Math. Model. 90 (2021), 466–473. https://doi.org/10.1016/j.apm.2020.08.057.

[7] C. Ji, D. Jiang, Threshold Behaviour of a Stochastic SIR Model, Appl. Math. Model. 38 (2014), 5067–5079. https://doi.org/10.1016/j.apm.2014.03.037.

[8] Y. Chen, P. Lu, C. Chang, T. Liu, A Time-Dependent SIR Model for COVID-19 with Undetectable Infected Persons, IEEE Trans. Netw. Sci. Eng. 7 (2020), 3279–3294. https://doi.org/10.1109/TNSE.2020.3024723.

[9] B. Dubey, P. Dubey, U.S.S. Dubey, Role of Media and Treatment on an SIR Model, Nonlinear Anal. Model. Control 21 (2016), 185–200. https://doi.org/10.15388/NA.2016.2.3.

[10] K. Zhu, L. Ying, Information Source Detection in the SIR Model: A Sample-Path-Based Approach, IEEE/ACM Trans. Netw. 24 (2016), 408–421. https://doi.org/10.1109/TNET.2014.2364972.

[11] M. Saberi, H. Hamedmoghadam, M. Ashfaq, S.A. Hosseini, Z. Gu, et al., A Simple Contagion Process Describes Spreading of Traffic Jams in Urban Networks, Nat. Commun. 11 (2020), 1616. https://doi.org/10.1038/s41467-020-15353-2.

[12] J. Wu, Z. Gao, H. Sun, Simulation of Traffic Congestion with SIR Model, Mod. Phys. Lett. B 18 (2004), 1537–1542. https://doi.org/10.1142/s0217984904008031.

[13] C. Pu, S. Li, X. Yang, Z. Xu, Z. Ji, et al., Traffic-driven SIR Epidemic Spreading in Networks, Physica A 446 (2016), 129–137. https://doi.org/10.1016/j.physa.2015.11.028.

[14] Y. Chen, J. Mao, Z. Zhang, H. Huang, W. Lu, et al., A Quasi-Contagion Process Modeling and Characteristic Analysis for Real-World Urban Traffic Network Congestion Patterns, Physica A 603 (2022), 127729. https://doi.org/10.1016/j.physa.2022.127729.

[15] R. Herdiana, Z.A. Rafsanjani, R.H. Tjahjana, Y.A. Erlangga, M.F. Ansori, Analysis of SIR Model with Optimal Control Strategy for a Simple Traffic Congestion Process, Commun. Math. Biol. Neurosci. 2024 (2024), 6. https://doi.org/10.28919/cmbn/8336.

[16] E. Harahap, P. Purnamasari, N. Saefudin, A. Nurrahman, D. Darmawan, et al., A Design Simulation of Traffic Light Intersection Using SimEvents MATLAB, J. Phys.: Conf. Ser. 1375 (2019), 012042. https://doi.org/10.1088/1742-6596/1375/1/012042.

[17] T.K. Kar, S. Jana, A Theoretical Study on Mathematical Modelling of an Infectious Disease with Application of Optimal Control, Biosystems 111 (2013), 37–50. https://doi.org/10.1016/j.biosystems.2012.10.003.

[18] A. Korobeinikov, G.C. Wake, Lyapunov Functions and Global Stability for SIR, SIRS, and SIS Epidemiological Models, Appl. Math. Lett. 15 (2002), 955–960. https://doi.org/10.1016/s0893-9659(02)00069-1.

[19] O. Diekmann, J.A.P. Heesterbeek, J.A.J. Metz, On the Definition and the Computation of the Basic Reproduction Ratio R_0 in Models for Infectious Diseases in Heterogeneous Populations, J. Math. Biol. 28 (1990), ahead of print. https://doi.org/10.1007/bf00178324.

[20] O. Diekmann, J.A.P. Heesterbeek, Mathematical Epidemiology of Infectious Diseases: Model Building, Analysis and Interpretation, Wiley, 2000.

[21] P. van den Driessche, J. Watmough, Reproduction Numbers and Sub-threshold Endemic Equilibria for Compartmental Models of Disease Transmission, Math. Biosci. 180 (2002), 29–48. https://doi.org/10.1016/s0025-5564(02)00108-6.

[22] C. Vargas-De-León, On the Global Stability of SIS, SIR and SIRS Epidemic Models with Standard Incidence, Chaos Solit. Fractals 44 (2011), 1106–1110. https://doi.org/10.1016/j.chaos.2011.09.002.

[23] Z. Hu, Z. Teng, L. Zhang, Stability and Bifurcation Analysis in a Discrete SIR Epidemic Model, Math. Comput. Simul. 97 (2014), 80–93. https://doi.org/10.1016/j.matcom.2013.08.008.

[24] J. La Salle, S. Lefschetz, Stability by Lyapunov's Direct Method, Academic Press, 1961.

[25] M.F. Emzir, M.J. Woolley, I.R. Petersen, Stability Analysis of Quantum Systems: A Lyapunov Criterion and an Invariance Principle, Automatica 146 (2022), 110660. https://doi.org/10.1016/j.automatica.2022.110660.